Day-ahead Voltage-stability-constrained Network Topology Optimization with Uncertainties

Dingli Guo, Lei Wang, Ticao Jiao, Ke Wu, and Wenjing Yang

***Abstract*—A day-ahead voltage-stability-constrained network topology optimization (DVNTO) problem is proposed to find the day-ahead topology schemes with the minimum number of operations (including line switching and bus-bar splitting) while ensuring the sufficient hourly voltage stability margin and the engineering operation requirement of power systems. The AC continuation power flow and the uncertainty from both renewable energy sources and loads are incorporated into the formulation. The proposed DVNTO problem is a stochastic, large-scale, nonlinear integer programming problem. To solve it tractably, a tailored three-stage solution methodology, including a scenario generation and reduction stage, a dynamic period partition stage, and a topology identification stage, is presented. First, to address the challenges posed by uncertainties, a novel problem-specified scenario reduction process is proposed to obtain the representative scenarios. Then, to obtain the minimum number of necessary operations to alter the network topologies for the next 24-hour horizon, a dynamic period partition strategy is presented to partition the hours into several periods according to the hourly voltage information based on the voltage stability problem. Finally, a topology identification stage is performed to identify the final network topology scheme. The effectiveness and robustness of the proposed three-stage solution methodology under different loading conditions and the effectiveness of the proposed partition strategy are evaluated on the IEEE 118-bus and 3120-bus power systems.**

***Index Terms*—Network topology optimization, static voltage stability, line switching, bus-bar splitting, renewable energy sources.**

I. Introduction

ONE of the distinctive features of modern power systems is the growing penetration of renewable energy sources into power systems, which has the notable impacts on the secure and stable operation of power systems [1]. It has been reported that power systems tend to operate near the stability boundary due to the increasing load demand and the intense uncertainty driven by the volatility and randomness of renewable energy sources [2], [3]. Coupled with that comes from loads, the uncertainties from both renewable energy sources and loads increase the complexities of the analysis and control of power systems. Hence, it is urgent to promote effective preventive controls to ensure the security and stability of power systems.

Various controls have been suggested and investigated, such as var sources [4], [5] and load shedding [6], to improve the static voltage stability of power systems. Network topology optimization (NTO) has been recognized as another promising control for operators to ensure the secure, economic, and stable operation of power systems. In distribution systems, the network topology can be changed by the tie switches and the sectionalizing switches, which have received significant attention since 1975 [7]. For transmission systems, the common ways to alter the network topology include transmission line switching-in, line switching-out, and bus-bar splitting [8]. Many researchers have investigated the applications of transmission NTO for alleviating voltage violation [9], [10], relieving congestion [11], [12], reducing cost [13], [14], and improving stability [15]-[17]. To examine effects of line switching on improving the static voltage stability of power systems, a security-constrained AC optimal power flow (OPF) model is presented to calculate the load margin to static voltage stability limits with the optimal line switching by a Benders-decomposition method [15], which concludes that optimal switching lines can increase the load margin. In addition, according to our previous research in [16] and [17], bus-bar splitting and line switching can also increase the load margin to static voltage stability limits, including two types of static bifurcations: saddle-node bifurcation (SNB) and structure-induced bifurcation (SIB).

To extend the NTO, many researchers have incorporated the NTO into the optimization operations of power systems. For example, a day-ahead scheduling model while considering transmission switching is proposed to restrict short-circuit current and minimize system operation cost [18]. In [19], the corrective NTO with contingency is presented to reduce the number of cases with constraint violations and improve the reserve deliverability. An optimal operational scheduling framework with the NTO is proposed to minimize the day-ahead total operation costs in the distribution management system [20]. In [21], the NTO and dynamic thermal rating are incorporated in the network-constrained

Manuscript received: September 18, 2023; revised: November 4, 2023; accepted: November 10, 2023. Date of CrossCheck: November 10, 2023. Date of online publication: December 12, 2023.

This work was supported by the National Natural Science Foundation of China (No. 52377109), the Natural Science Foundation of Shandong Province (No. ZR2022ME187), and the Taishan Scholar Project of Shandong Province (No. TSQN202306191).

D. Guo, L. Wang (corresponding author), T. Jiao, K. Wu, and W. Yang are with the School of Electrical and Electronic Engineering, Shandong University of Technology, Zibo 255000, China (e-mail: guodingli0106@163.com; wanglei@sdut.edu.cn; ticaojiao@gmail.com; wukesdut@163.com; 3116562416@qq.com).

DOI: 10.35833/MPCE.2023.000673

unit commitment framework in day-ahead scheduling problems to reduce total dispatch and wind power spillage costs. In [22], a day-ahead stochastic optimal transmission switching problem is formulated considering load, wind, and solar generation uncertainties. In [23], the transmission switching is applied in the day-ahead scheduling problem to reduce wind curtailment and minimize the generation costs of thermal units.

Besides the cost and the security constraints, the voltage stability constraints have been considered in the NTO problems. The linearized indicators are popularly employed to measure the voltage stability degree in the NTO problem, e. g., the L-indicator [24], the fast voltage stability index [25], and the line-power-based index [26], [27]. The advantage of these indexes is that the computation complexity can be reduced because of the linear property; however, these indexes cannot reflect the impacts of uncertainties and power injection variations on the voltage stability caused by fluctuations of generations and loads. From our previous studies, the impacts are strongly nonlinear and cannot be ignored for the voltage stability problem [28]. Therefore, it is an issue to model the uncertainty and add the detailed nonlinear voltage stability index into the NTO problem to describe the nonlinear impacts of uncertainties and power injection variations.

Moreover, from the operational viewpoint, a practical issue is that too many operations for NTO are undesirable because of the potential risks for the secure operation of power systems and the heavy work for system operators. Hence, a limited/minimal number of operations is crucial and more practical for the online application of the NTO [29]. For the day-ahead NTO problem, the time period partition is an essential technique to identify similar periods and cluster them into several periods, which is used in this study to partition time periods to reduce the the number of operations for the NTO. To decrease the computational burden due to the whole time horizon, the fuzzy C-means (FCM) clustering method is used to partition time periods into several adjacent periods based on different indexes, e. g., the operation cost [30], the intrinsic similarity of load data [31], and the line loss [32], and then the dynamic network reconfiguration problem is transformed into multiple static network reconfiguration problems. But for the day-ahead NTO with the voltage stability constraint problem, the information at the voltage collapse point should be considered to perform the period partition.

This paper focuses on minimizing the number of NTO schemes required while ensuring that the static voltage stability achieves the desired stability level. To this end, a novel formulation called day-ahead voltage-stability-constrained network topology optimization (DVNTO) is proposed in this paper, which considers the inherent uncertainty of renewable energy sources and loads. It is very challenging for the proposed DVNTO problem to find the best NTO scheme from the large number of NTO candidate schemes. Hence, an effective and fast solution methodology is needed. The main contributions of this paper are as follows.

1) The comprehensive NTO schemes (including line switching-in, line switching-out, and bus-bar splitting) are incorporated into the DVNTO problem to demonstrate the effect of line switching and bus-bar splitting on improving the voltage stability. To flexibly mimic the NTO schemes, a general NTO model is presented, which is suitable for fast screening the NTO candidate schemes.

2) A DVNTO problem formulation is proposed to find the day-ahead NTO schemes with a minimal number of operations. The AC continuation power flow constraints, AC power flow constraints, and uncertainties from renewable energy sources and load fluctuations are incorporated in the formulation, instead of the linearized constraints.

3) A problem-specified scenario construction method is presented to address the nonlinear impacts of uncertainties on the voltage stability margin.

4) A three-stage methodology is developed to solve the proposed DVNTO problem, which involves the scenario generation and reduction stage, dynamic period partition stage, and topology identification stage.

The remainder of this paper is organized as follows. The modeling of topology optimization and uncertainty are described in Section II. The DVNTO problem formulation and the solution methodology are presented in Section III and Section IV, respectively. Numerical studies on the IEEE 118-bus and 3120-bus power systems are extensively analyzed in Section V. Section VI concludes this paper and the possible future work.

II. Modeling of Topology Optimization and Uncertainty

A. A General NTO Model

Both line switching and bus-bar splitting are considered as the possible controls for the NTO in this paper, which can be illustrated by Fig. 1.

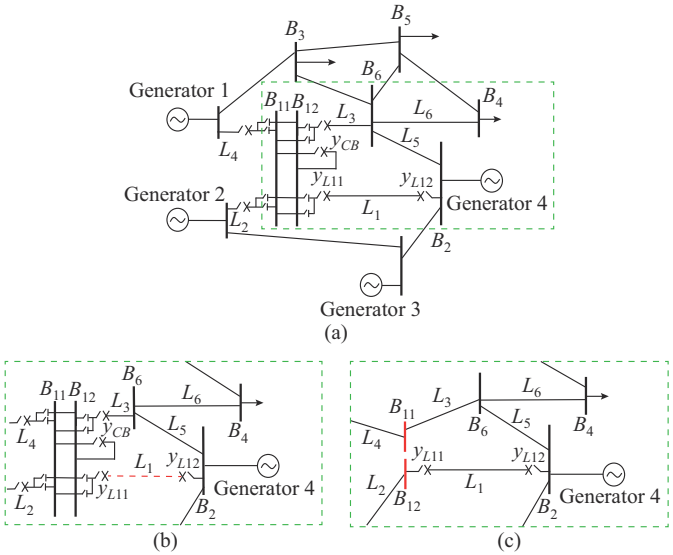

Fig. 1. Illustration of NTO. (a) Topolgy before NTO. (b) Line switching-out. (c) Bus-bus splitting.

Four line branches are connected on the bus-bars B_{11} and B_{12}. The possible controls include line switching (line L_1 is

switched into service in Fig. 1(a) and line L_1 is switched out of service in Fig. 1(b)) and bus-bar splitting (the bus-bar layout of the substation can be changed by circuit breakers; for example, in Fig. 1(a), the bus-bars B_{11} and B_{12} are connected when the circuit breaker y_{CB} is closed; otherwise, bus-bars B_{11} and B_{12} are split and a new layout is constructed). There are six potential NTO schemes for bus-bars B_{11} and B_{12} in this example, in which Fig. 1(c) is one of them.

How to flexibly mimic all the possible schemes and identify the optimal NTO scheme quickly from a lot of candidates is a very challenging task. To flexibly mimic the changes of topologies, a general NTO model is proposed, inspired by Ward equivalent theory in this paper. Taking the network shown in Fig. 2 as an example, the altered part of the network topology due to NTO is defined as the internal subsystem with the boundary buses B (i.e., B_1, B_2, B_3, B_4, and B_5) and the internal buses R (i.e., R_1 and R_2). The other part of the network topology is defined as the external subsystem with the external buses E (i.e., E_1, E_2, E_3, and E_4). In Fig. 2, the red line represents the line that is switched out after NTO. According to the Ward equivalent theory, the internal subsystem can be converted into a mesh network with the boundary buses as vertices.

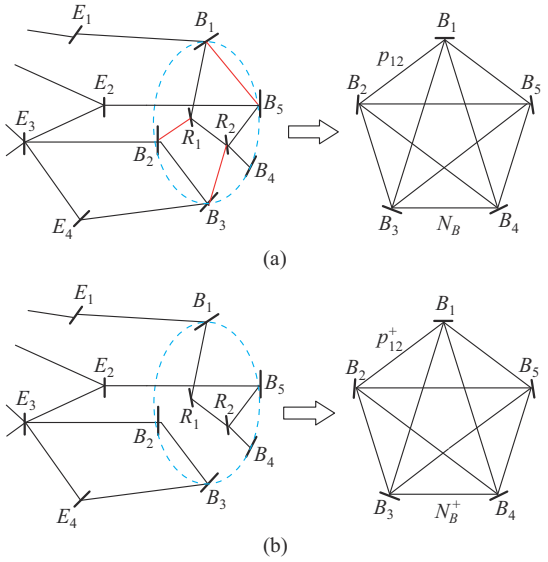

Fig. 2. Illustration of proposed general NTO model. (a) Before NTO. (b) After NTO.

Before the NTO, the voltage equation of the power system can be described as:

$$\begin{bmatrix} \boldsymbol{Y}_{RR} & \boldsymbol{Y}_{RB} & \boldsymbol{0} \\ \boldsymbol{Y}_{BR} & \boldsymbol{Y}_{BB} & \boldsymbol{Y}_{BE} \\ \boldsymbol{0} & \boldsymbol{Y}_{EB} & \boldsymbol{Y}_{EE} \end{bmatrix} \begin{bmatrix} \dot{\boldsymbol{V}}_R \\ \dot{\boldsymbol{V}}_B \\ \dot{\boldsymbol{V}}_E \end{bmatrix} = \begin{bmatrix} \dot{\boldsymbol{I}}_R \\ \dot{\boldsymbol{I}}_B \\ \dot{\boldsymbol{I}}_E \end{bmatrix} \tag{1}$$

where $\boldsymbol{Y}_{RR}$, $\boldsymbol{Y}_{BB}$, and $\boldsymbol{Y}_{EE}$ are the self-admittance matrices of the internal buses, boundary buses, and external buses, respectively; $\boldsymbol{Y}_{RB}$, $\boldsymbol{Y}_{BE}$, $\boldsymbol{Y}_{BR}$, and $\boldsymbol{Y}_{EB}$ are the mutual admittance matrices; $\dot{\boldsymbol{V}}_R$, $\dot{\boldsymbol{V}}_B$, and $\dot{\boldsymbol{V}}_E$ are the matrices of the bus voltages; and $\dot{\boldsymbol{I}}_R$, $\dot{\boldsymbol{I}}_B$, and $\dot{\boldsymbol{I}}_E$ are the matrices of injection currents. Eliminating the first line in (1) by the Gaussian elimination method, the internal subsystem can be represented as an equivalent network N_B (i.e., the mesh network in Fig. 2(a)) with the admittance $\tilde{\boldsymbol{Y}}_{BB}$, which is connected to the external subsystem by the boundary buses.

$$\begin{bmatrix} \tilde{\boldsymbol{Y}}_{BB} & \boldsymbol{Y}_{BE} \\ \boldsymbol{Y}_{EB} & \boldsymbol{Y}_{EE} \end{bmatrix} \begin{bmatrix} \dot{\boldsymbol{V}}_B \\ \dot{\boldsymbol{V}}_E \end{bmatrix} = \begin{bmatrix} \dot{\boldsymbol{I}}_B \\ \dot{\boldsymbol{I}}_E \end{bmatrix} \tag{2a}$$

$$\tilde{\boldsymbol{Y}}_{BB} = \boldsymbol{Y}_{BB} - \boldsymbol{Y}_{BR}\boldsymbol{Y}_{RR}^{-1}\boldsymbol{Y}_{RB} \tag{2b}$$

where $\tilde{\boldsymbol{Y}}_{BB}$ is the admittance matrix of the equivalent internal subsystem.

After the NTO, the topology of the internal subsystem is changed, whereas the boundary buses and the external subsystem remain unchanged. Hence, the voltage equation of the power system after the NTO can be described as:

$$\begin{bmatrix} \boldsymbol{Y}_{RR}^{+} & \boldsymbol{Y}_{RB}^{+} & \boldsymbol{0} \\ \boldsymbol{Y}_{BR}^{+} & \boldsymbol{Y}_{BB}^{+} & \boldsymbol{Y}_{BE} \\ \boldsymbol{0} & \boldsymbol{Y}_{EB} & \boldsymbol{Y}_{EE} \end{bmatrix} \begin{bmatrix} \dot{\boldsymbol{V}}_R^{+} \\ \dot{\boldsymbol{V}}_B^{+} \\ \dot{\boldsymbol{V}}_E \end{bmatrix} = \begin{bmatrix} \dot{\boldsymbol{I}}_R^{+} \\ \dot{\boldsymbol{I}}_B^{+} \\ \dot{\boldsymbol{I}}_E \end{bmatrix} \tag{3}$$

where the superscript "+" denotes the elements changed due to the NTO. Similarly, the internal subsystem can be represented by a new mesh network N_B^+ shown in Fig. 2(b) with the admittance matrix $\tilde{\boldsymbol{Y}}_{BB}^{+}$, i.e.,

$$\begin{bmatrix} \tilde{\boldsymbol{Y}}_{BB}^{+} & \boldsymbol{Y}_{BE} \\ \boldsymbol{Y}_{EB} & \boldsymbol{Y}_{EE} \end{bmatrix} \begin{bmatrix} \dot{\boldsymbol{V}}_B^{+} \\ \dot{\boldsymbol{V}}_E^{+} \end{bmatrix} = \begin{bmatrix} \dot{\boldsymbol{I}}_B^{+} \\ \dot{\boldsymbol{I}}_E^{+} \end{bmatrix} \tag{4a}$$

$$\tilde{\boldsymbol{Y}}_{BB}^{+} = \boldsymbol{Y}_{BB}^{+} - \boldsymbol{Y}_{BR}^{+}(\boldsymbol{Y}_{RR}^{+})^{-1}\boldsymbol{Y}_{RB}^{+} \tag{4b}$$

Hence, the difference between network topologies before and after the NTO can be equivalent to the admittance change of two mesh networks N_B and N_B^+, i.e.,

$$\Delta\boldsymbol{Y} = \tilde{\boldsymbol{Y}}_{BB}^{+} - \tilde{\boldsymbol{Y}}_{BB} \tag{5}$$

The proposed model is suitable for any switching action such as the NTO and shunt switching, and supports the fast-screening task to screen out those invalid NTO schemes by a linearized method. The detailed steps are summarized in Section IV-B.

B. Uncertainty Characterization and Scenario Generation

In this paper, the uncertainties are modeled by scenario-based methods. R-vine Copula method is used to fit the correlations according to the historical data to model the spatial correlations among renewable energy sources. Assume that an available prediction technique can provide day-ahead predicted loads and renewable energy sources. The hourly prediction errors of load demands and the outputs of renewable energy sources can be described by the normally-distributed random variables. Assume that the standard deviations are $\sigma_{R,i,t}^2$ and $\sigma_{L,j,t}^2$ for the renewable energy source on load buses i and j at the t^{th} hour, respectively, and the (predicted) mean values are $M_{R,i,t}$ and $M_{L,i,t}$, the outputs of renewable energy sources and load demands on bus i can be represented as scenario sets $S_{i,t}^R$ ($S_{i,t}^R \sim N(M_{R,i,t}, \sigma_{R,i,t}^2)$) and $S_{i,t}^L$ ($S_{i,t}^L \sim N(M_{L,i,t}, \sigma_{L,i,t}^2)$), respectively. According to the previous studies in [28], the joint scenarios of renewable energy sources and loads should be used to describe the nonlinear characteristic between the scenarios and the voltage stability, i.e., the joint scenario set $SS_{i,t}$ on bus i at the t^{th} hour is the Cartesian product of the scenario set $S_{i,t}^R$ and the scenario set $S_{i,t}^L$.

$$SS_{i,t}=S_{i,t}^{R}\times S_{i,t}^{L}=\left\{\left\langle s_{R,i,t},s_{L,i,t}\right\rangle \,\middle|\, s_{R,i,t}\in S_{i,t}^{R}\wedge s_{L,i,t}\in S_{i,t}^{L}\right\} \quad (6)$$

where $s_{R,i,t}$ and $s_{L,i,t}$ are the elements of the sets $S_{i,t}^{R}$ and $S_{i,t}^{L}$, respectively. Then, all the day-ahead scenarios of renewable energy sources and loads can be composed, for example, the k^{th} scenario Z_k can be composed by:

$$Z_k=\{z_{1,k},z_{2,k},\ldots,z_{t,k},\ldots,z_{24,k}\} \quad (7a)$$

$$z_{t,k}=\{s_{R,1,t},s_{R,2,t},\ldots,s_{R,n,t},s_{L,1,t},s_{L,2,t},\ldots,s_{L,n,t}\} \quad (7b)$$

where n is the total number of buses of the power system.

III. DVNTO Problem Formulation

The proposed problem aims to determine the day-ahead optimized network topologies altered by the minimal number of necessary actions to ensure enough hourly voltage stability margin up to a desired value λ_{th} and the engineering operation requirements of power systems. Hence, the proposed problem formulation can be described as:

$$\min\sum_{t=1}^{24}NE(N_t-N_{t-1}) \quad (8)$$

s.t.

$$f_{z_{t,k}}^{N_t}(\boldsymbol{x}_{z_{t,k}},\lambda_{z_{t,k}},\boldsymbol{d}_{z_{t,k}})=0 \quad \forall z_{t,k}\in Z_k \quad (9)$$

$$g_{z_{t,k}}^{N_t}(\boldsymbol{x}_{z_{t,k}},\boldsymbol{d}_{z_{t,k}})=0 \quad \forall z_{t,k}\in Z_k \quad (10)$$

$$\lambda_{z_{t,k}}\geq\lambda_{th} \quad \forall z_{t,k}\in Z_k \quad (11)$$

$$V_{i,\min}\leq V_{i,z_{t,k}}\leq V_{i,\max} \quad \forall i\in B_n \quad (12a)$$

$$|S_{(i,j),z_{t,k}}|\leq S_{(i,j),\max} \quad \forall i,j\in B_n \quad (12b)$$

where N_{t-1} and N_t are the network topologies at the $(t-1)^{\text{th}}$ and t^{th} hour, respectively; $NE(\cdot)$ maps the difference of network topologies, i. e., the needed number of line switching and bus-bar splitting to alter the network topology from N_{t-1} to N_t; $f_{z_{t,k}}^{N_t}$ and $g_{z_{t,k}}^{N_t}$ denote the AC continuation power flow equation and the AC power flow equation in the scenario $z_{t,k}$ and the topology N_t, respectively; $\boldsymbol{x}_{z_{t,k}}$ and $\lambda_{z_{t,k}}$ are the voltage vector and the load margin in the scenario $z_{t,k}$, respectively; $V_{i,z_{t,k}}$ is the voltage magnitude of bus i in the scenario $z_{t,k}$; $V_{i,\min}$ and $V_{i,\max}$ are the lower and upper limits of the voltage magnitude of bus i in the scenario $z_{t,k}$, respectively; B_n is the set of buses; $S_{(i,j),z_{t,k}}$ and $S_{(i,j),\max}$ are the apparent power of line i-j in the scenario $z_{t,k}$ and its limit, respectively; and $\boldsymbol{d}_{z_{t,k}}$ is the power injection variation in the scenario $z_{t,k}$, specified by the rescheduling active and reactive power generations, the load demand, and their uncertainties.

The objective function (8) maps the minimal number of required operations to change the network topologies for the day-ahead power system. Constraints (9) and (10) are the AC nonlinear continuation power flow equations and the AC power flow equations of the day-ahead power system, respectively. Constraint (11) is the hourly load margin requirement. Constraints (12a) and (12b) represent the operational engineering constraints, including the voltage magnitude limit constraint (12a) and the thermal limit constraint (12b).

The nonlinear impact of the power injection variations on the load margin to static voltage stability limit has been studied in [33]. Hence, the change in the power injection variation due to uncertainties should be considered in the proposed problem. The variation of the active power injection at the t^{th} hour can be illustrated by the 2-D space in Fig. 3, where $\boldsymbol{P}_{z_{t,k}}$ and $\boldsymbol{P}_{z_{t+1,k}}$ are the active power injections of the bus in the scenarios $z_{t,k}$ and $z_{t+1,k}$, respectively. Hence, the variation of the active power injection is $\boldsymbol{d}_{\boldsymbol{P}_{z_{t,k}}}=\boldsymbol{P}_{z_{t+1,k}}-\boldsymbol{P}_{z_{t,k}}$. Similarly, the variation of the reactive power injection at the t^{th} hour is $\boldsymbol{d}_{\boldsymbol{Q}_{z_{t,k}}}=\boldsymbol{Q}_{z_{t+1,k}}-\boldsymbol{Q}_{z_{t,k}}$, where $\boldsymbol{Q}_{z_{t,k}}$ and $\boldsymbol{Q}_{z_{t+1,k}}$ are the reactive power injections of the bus in the scenarios $z_{t,k}$ and $z_{t+1,k}$, respectively. Hence, the power injection variation in the scenario $z_{t,k}$ is $\boldsymbol{d}_{z_{t,k}}=[\boldsymbol{d}_{P_{z_{t,k}}},\boldsymbol{d}_{Q_{z_{t,k}}}]^{\text{T}}$.

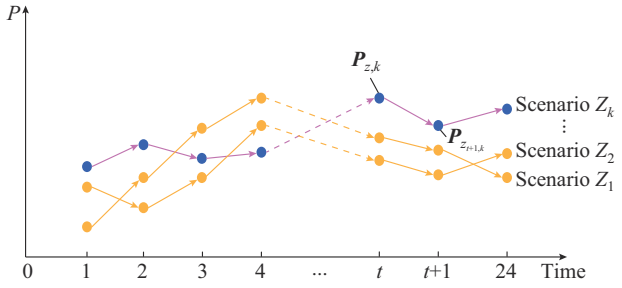

Fig. 3. Illustration of variation of active power injection.

IV. Solution Methodology

A three-stage methodology is presented to solve the DVNTO problem, whose framework is shown in Fig. 4, which includes the scenario generation and reduction (stage I), the dynamic period partition (stage II), and the topology identification (stage III). In Fig. 4, t_e is the end hour of the first period. The necessary inputs include the predicted renewable energy sources and loads, the hourly generation, the maintenance schedules, and the desired voltage stability margin λ_{th}.

A. Stage I

This stage aims to employ the scenario generation method in Section II-B to model the uncertainties and obtain the RS set.

The critical issue for the scenario-based modeling method is how to reduce the number of scenarios to reduce the computation burden from a large number of scenarios. According to our experience, to obtain RSs and avoid the mis-elimination of the extreme scenarios, the scenarios should be reduced according to the impact of scenarios on the load margin instead of the distances among the scenarios. Therefore, a tailored scenario reduction method is presented in this paper, whose steps are summarized as follows.

Step 1: cluster all the generated joint scenarios in Section II-B into groups according to the distance between scenario pairs and identify the central scenario of each group. The distance $D_{(k,k')}$ between the scenarios Z_k and $Z_{k'}$ is:

$$D_{(k,k')}=\sqrt{\frac{1}{24}\sum_{t=1}^{24}\left\|z_{t,k}-z_{t,k'}\right\|^2} \quad (13)$$

Step 2: choose a scenario group and compute the hourly load margin $\lambda_{Z_0}=\{\lambda_{z_{1,0}},\lambda_{z_{2,0}},\ldots,\lambda_{z_{t,0}},\ldots,\lambda_{z_{24,0}}\}$ of the central sce-

nario Z_0 of this group and the hourly non-zero left eigenvector corresponding to the hourly zero eigenvalue of the Jacobian matrix at the bifurcation point.

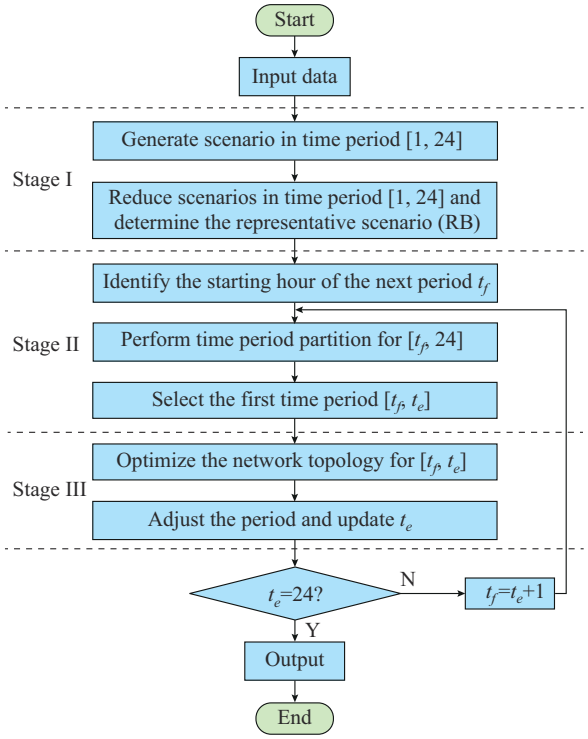

Fig. 4. Framework of proposed methodology.

Step 3: estimate the hourly load margins of the k^{th} scenario within this group by (14) and (15).

$$\lambda_{z_{t,k}}=\lambda_{z_{t,0}}+\Delta\lambda_{z_{t,k}}^{z_{t,0}}=\lambda_{z_{t,0}}-\tilde{\boldsymbol{\omega}}_{z_{t,0}}\frac{\partial f_{z_{t,0}}^{N_t}}{\partial z_{t,k}}(z_{t,0}-z_{t,k}) \tag{14}$$

$$\tilde{\boldsymbol{\omega}}_{z_{t,0}}=\boldsymbol{\omega}_{z_{t,0}}\Big/\left(\boldsymbol{\omega}_{z_{t,0}}\frac{\partial f_{z_{t,0}}^{N_t}}{\partial\lambda_{z_{t,0}}}\right)\quad t\in\{1,2,\ldots,24\} \tag{15}$$

where $\Delta\lambda_{z_{t,k}}^{z_{t,0}}$ is the load margin change due to the difference of the scenario $z_{t,0}$ and the scenario $z_{t,k}$; $f_{z_{t,0}}^{N_t}$ denotes the AC continuation power flow equation in the scenario $z_{t,0}$ and the topology N_t; and $\boldsymbol{\omega}_{z_{t,0}}$ is the non-zero eigenvalue of the Jacobian matrix of $f_{z_{t,0}}^{N_t}$ at the bifurcation point. Repeat *Step 3* until the hourly load margins of all the scenario groups are estimated.

Step 4: cluster all the scenarios into groups according to the distance of the estimated load margins by (16). The distance of load margins $D_{\lambda(k,k')}$ between two scenarios Z_k and $Z_{k'}$ is:

$$D_{\lambda(k,k')}=\sqrt{\frac{1}{24}\sum_{t=1}^{24}\left\|\lambda_{z_{t,k}}-\lambda_{z_{t,k'}}\right\|^2} \tag{16}$$

Select the scenario with minimal load margin of each group as the RS to form the RS set $RSS=\{RS_1,RS_2,\ldots,RS_k,\ldots,RS_r\}$, where RS_k is the k^{th} RS and $RS_k=\{rs_{1,k},rs_{2,k},\ldots,rs_{t,k},\ldots,rs_{24,k}\}$, $rs_{t,k}$ is the hourly scenario at the t^{th} hour of RS_k, and r is the number of RSs.

B. Stage II

The aim of this stage is to partition the hours into several periods according to the worst scenario RS_d determined by the following problem (17), which is proposed to determine RS_d and identify the first hour t_f with the violation of constraint (11). The following period partition will be performed from t_f.

$$d=\arg\max_{1\le i\le r}\sum_{t=t_f}^{24}a_{rs_{t,i}} \tag{17a}$$

s.t.

$$a_{rs_{t,i}}=\begin{cases}1 & \lambda_{rs_{t,i}}<\lambda_{th}\\ 0 & \text{else}\end{cases} \tag{17b}$$

where d denotes the d^{th} RS of RSS; $\lambda_{rs_{t,i}}$ is the load margin of power system in the scenario $rs_{t,i}$; and $a_{rs_{t,i}}$ is an integer variable, and if $\lambda_{rs_{t,i}}<\lambda_{th}$, $a_{rs_{t,i}}=1$, otherwise $a_{rs_{t,i}}=0$.

To partition the hours into periods, the distinctive feature of this paper is that the voltage changes between the bifurcation point and the power flow point are used as the clustered index and a cluster validity index V_{OSK} is proposed to evaluate partition results. For bus i, the change of voltage magnitude in the worst scenario $RS_d=\{rs_{1,d},rs_{2,d},\ldots,rs_{t,d},\ldots,rs_{24,d}\}$ is:

$$\Delta V_{rs_{t,d},i}=\left(V_{rs_{t,d},i}^{0}-V_{rs_{t,d},i}^{B}\right)\Big/V_{rs_{t,d},i}^{0} \tag{18}$$

where $V_{rs_{t,d},i}^{0}$ and $V_{rs_{t,d},i}^{B}$ are the voltage magnitudes of bus i at the operation point and the bifurcation point at the t^{th} hour in the worst scenario $rs_{t,d}$, respectively. We use a P-V curve shown in Fig. 5 to illustrate the bifurcation point (i.e., the nose point) and the load margin to static voltage stability limit (i.e., the distance between the power flow point and bifurcation point). $\lambda_{rs_{t,d}}$ is the load margin of power system in the scenario $rs_{t,d}$. Then, the following structure of the variables $\boldsymbol{W}_{RS_d,t}$ for the t^{th} hour can be obtained:

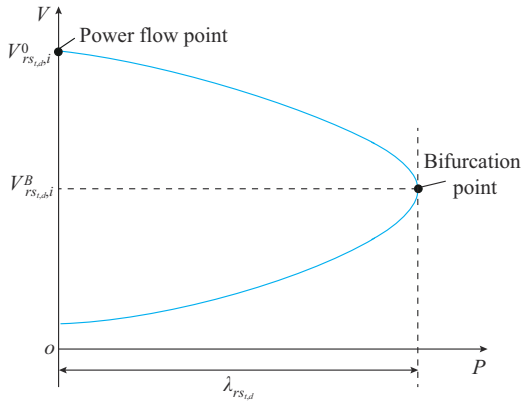

Fig. 5. P-V curve in scenario $rs_{t,d}$ at the t^{th} hour.

$$\boldsymbol{W}_{RS_d,t}=[\Delta V_{rs_{t,d},1}\quad\Delta V_{rs_{t,d},2}\quad\ldots\quad\Delta V_{rs_{t,d},n}\quad t]^{\mathrm{T}}\quad t=\{t_f,t_f+1,\ldots,24\} \tag{19}$$

To partition the hours into several intervals, the FCM cluster method is employed with the following objective function in this paper [34]:

$$\min J_m(\boldsymbol{U},\boldsymbol{H})=\min\sum_{t=t_f}^{24}\sum_{j=1}^{c}\mu_{t,j}^{m}\left\|\boldsymbol{W}_{RS_d,t}-\boldsymbol{v}_j\right\|^2 \tag{20}$$

where c is the number of clusters; $m\in[1,\infty)$ is a parameter controlling the fuzziness of the clustering procedure; $\mu_{t,j}\in[0,1]$ is the membership degree of $\boldsymbol{W}_{RS_d,t}$ to the cluster $\boldsymbol{v}_j$; $\boldsymbol{U}=(\mu_{t,j})$ is the membership matrix; and $\boldsymbol{H}=\{\boldsymbol{v}_1,\boldsymbol{v}_2,\ldots,\boldsymbol{v}_j,\ldots,\boldsymbol{v}_C\}$ is the output of the cluster center.

A vital point of the FCM cluster method is that the number of clusters and the fuzzy clustering coefficient must be specified in advance. Several research studies, e. g., [35], have provided the recommended range regarding the clustering fuzzy coefficient. In this paper, the solution of the optimal fuzzy coefficient is carried out with $2\le m\le 3$. To obtain a high-quality period partitioning result, a comprehensive validity index V_{OSK} is proposed in (22) to validate the quality of the partition in the paper. When V_{OSK} reaches its minimal value, the optimal cluster number c_{opt} [36] - [38] and the fuzzy coefficient m_{opt} are determined.

$$(c_{opt},m_{opt})=\arg\min_{2\le c\le c_{\max},2\le m\le 3}V_{OSK} \tag{21}$$

$$V_{OSK}=w_{V_{OS}}V_{OS}+w_{V_K}V_K \tag{22}$$

where $c_{\max}$ is the maximum number of clusters; $w_{V_{OS}}$ and w_{V_K} are the weights assigned to the effectiveness indexes V_{OS} and V_K by the entropy weight method [35], respectively; V_{OS} is a validity index to evaluate the cluster results based on overlap and separation [36]; and V_K is determined by the membership values and the geometric structure of the data set [37].

$$V_{OS}=\frac{Overlap(c,\boldsymbol{U})\Big/\max\limits_{2\le c\le c_{\max}}\{Overlap(c,\boldsymbol{U})\}}{Sep(c,\boldsymbol{U})\Big/\max\limits_{2\le c\le c_{\max}}\{Sep(c,\boldsymbol{U})\}} \tag{23}$$

$$V_K=\frac{\sum\limits_{t=t_f}^{24}\sum\limits_{j=1}^{c}\mu_{t,j}^{2}\left\|\boldsymbol{W}_{RS_d,t}-\boldsymbol{v}_j\right\|^2+\dfrac{1}{c}\sum\limits_{j=1}^{c}\left\|\boldsymbol{v}_j-\bar{\boldsymbol{v}}\right\|^2}{\min\limits_{j\ne k}\left\|\boldsymbol{v}_j-\boldsymbol{v}_k\right\|^2} \tag{24}$$

where $\bar{\boldsymbol{v}}=\sum_{t=t_f}^{24}\boldsymbol{W}_{RS_d,t}/(24-t_f+1)$; $Overlap(\cdot)$ is the overlap degree between clusters; and $Sep(\cdot)$ is the separation measure between two fuzzy clusters (please refer to [38] in details).

After this stage, the first period $[t_f,t_e]$ is identified and sent to the next stage.

C. Stage III

This stage is to determine the optimal topology that can increase the hourly load margins of the first period $[t_f,t_e]$ up to the desired requirement with the minimized number of operations by line switching and bus-bar splitting. To solve the problem, a "screening and ranking – verification" strategy is proposed to identify the most effective NTO schemes.

Step 1: screening and ranking.

In this step, the effective NTO schemes for the scenario $rs_{t_f,d}$ are screened from a large amount of NTO candidate schemes and then ranked by their load margins.

To fast evaluate the effect of each NTO candidate scheme on improving the load margin, a linear sensitivity-based method is employed and the sensitivity of the load margin on NTO scheme is derived to pre-screen all the NTO candidate schemes in the scenario $rs_{t_f,d}$, including line switching-in, line switching-out, and bus-bar splitting. According to the general NTO model proposed in Section II-A, the changes of topologies due to the NTO can be modeled as the changes of admittance matrices of the two mesh networks (5). Hence, the change of load margins due to the NTO in the scenario $rs_{t,d}$ can be estimated by (25) and (26).

$$\Delta\lambda_{NTO,rs_{t,d}}=\sum_{i=1}^{n_l-1}\sum_{j=i+1}^{n_l}\Delta\lambda_{ij,rs_{t,d}} \tag{25}$$

$$\Delta\lambda_{ij,rs_{t,d}}=-\boldsymbol{\omega}\frac{\partial f_{rs_{t,d}}^{N_t}}{\partial\boldsymbol{Y}}\Delta\boldsymbol{Y}\Big/(\boldsymbol{\omega}\boldsymbol{d}_{rs_{t,d}})\quad t=\{t_f,t_{f+1},\ldots,24\} \tag{26}$$

where n_l is the number of branches of the mesh networks N_B and N_B^+; $f_{rs_{t,d}}^{N_t}$ denotes the AC continuation power flow equation in the scenario $rs_{t,d}$ and the topology N_t; $\boldsymbol{\omega}$ is the nonzero eigenvalue of the Jacobian matrix of $f_{rs_{t,d}}^{N_t}$ at the bifurcation point; $\boldsymbol{Y}$ is the admittance matrix of the mesh network; $\Delta\boldsymbol{Y}$ is the admittance change of two mesh networks N_B and N_B^+ (5); and $\boldsymbol{d}_{rs_{t,d}}$ is the power injection variation in the scenario $rs_{t,d}$. After this step, all the NTO schemes with the nonnegative value (i.e., $\Delta\lambda_{NTO,rs_{t,d}}\ge 0$) are considered as the possible candidate schemes to improve the load margin.

To rank the reserved NTO schemes, the look-ahead margin estimation method [39] is used to estimate their load margins due to its accuracy and speed. The NTO schemes, whose load margin is greater than $0.9\lambda_{th}$, are ranked according to the estimated load margins by the look-ahead margin estimation method.

Step 2: verification.

Another feature of the proposed methodology is that multiple NTO schemes may be obtained in the above step. Hence, we can further identify the "best" NTO scheme that can meet the load margin requirement for all RSs with the largest period length. To identify the best one, a continuous power flow method is used to calculate the load margin for all RSs from t_f until the last hour that meets the load margin requirement is reached.

Our numerical studies show that: ① in some cases, the NTO schemes obtained in *Step 1* may not meet the load margin requirement (11) for the whole period $[t_f,t_e]$ under all the RSs; ② in some cases, the NTO schemes obtained in *Step 1* can also meet the load margin requirements (11) for the subsequent hours of the current period $[t_f,t_e]$ under all the RSs. Hence, in this step, the NTO scheme that can meet the load margin requirement (11) with the longest time period is the "optimal" solution. To this end, a dynamic period adjustment strategy, inspired by [36], is necessary to deal with the above situations, which can be illustrated in Fig. 6.

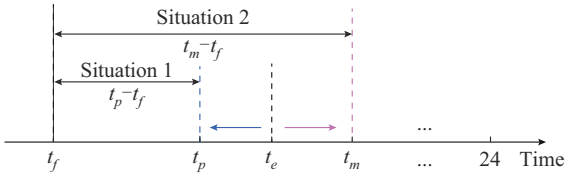

Fig. 6. Illustration of two situations in *Step 2*.

Situation 1: the obtained NTO schemes in *Step 1* are used to verify the load margin requirement (11) under each RS from the first hour t_f. The NTO scheme with the longest time period $[t_f, t_p]$ is the solution, and update $t_e = t_p$. t_p is the last hour of this period that the NTO scheme can meet the requirement of load margin (11).

Situation 2: the obtained NTO schemes in *Step 1* are used to verify the load margin requirement (11) for the subsequent hours until the last hour without violating (11) is met, and update $t_e = t_m$. t_m is the last hour outside the period $[t_f, t_e]$ that the NTO scheme can meet the requirement of load margin (11).

Based on the above process, the NTO scheme for the period $[t_f, t_e]$ is determined, and sent to the period $[t_e + 1, 24]$ as the new initial topology to perform the proposed methodology till the NTO schemes for 24 hours are determined.

V. Numerical Studies

The effectiveness of the proposed methodology, the proposed partition strategy, and the performance of the comprehensive NTO have been tested on IEEE 118-bus and 3120-bus power systems [40]. The actual historical data of renewable energy sources are from the International Renewable Energy Agency (IRENA) website [41], and the electric load data of 2022 are from the California Independent System Operator (CAISO) [42]. For comparison purposes, the following methods are designed to show the effectiveness of the proposed methodology.

1) Method M1: the method does not employ the proposed verification step.

2) Method M2: the method does not employ the proposed period partition step.

3) Method M3: the method conducts the period partition based on the net loads.

A. IEEE 118-bus Power System

Assume that 3 photovoltaic (PV) power stations are installed at buses 72, 73, and 74, and 3 wind generators are installed at buses 90, 91, and 92. The lower and upper bounds of bus voltage magnitudes are 0.94 p.u. and 1.06 p.u., respectively. The day-ahead active power and reactive power of loads are shown in Fig. 7. In this example, 177 transmission lines and 21 bus bars (292 splitting schemes) with more than 4 branches are considered as the candidates to alter the grid topology. Let $\lambda_{th} = 1.905$ p.u..

The outputs of the proposed methodology are as follows.

1) In stage I, a total of 1000 joint scenarios are generated and 4 RSs are obtained by the proposed scenario reduction method.

2) After stage II, the ineligible hourly load margins in the 4 RSs are listed in Table I, and RS 1 is the worst one. Hence, the period partition is performed in RS 1 and 6 time periods are obtained by the proposed partition strategy. The hourly load margins in the worst scenario and the 6 time periods are shown in Fig. 7.

3) In stage III, the NTO scheme with switching out the line 114 is determined as the best solution for the first period 01:00-06:00 and it can support the load margin requirement in this period. Hence, the solution for the first period is the topology with switching out the line 114.

TABLE I
Ineligible Load Margins in 4 RSs

RS 1		RS 2		RS 3		RS 4	
t	λ_t (p.u.)	t	λ_t (p.u.)	t	λ_t (p.u.)	t	λ_t (p.u.)
02:00	1.8412	02:00	1.8206	06:00	1.8531	02:00	1.8732
07:00	1.8313	06:00	1.8384	07:00	1.8623	07:00	1.8663
11:00	1.8642	17:00	1.8576	11:00	1.8035	17:00	1.8617
17:00	1.7785			17:00	1.8674	23:00	1.8524
23:00	1.7842						

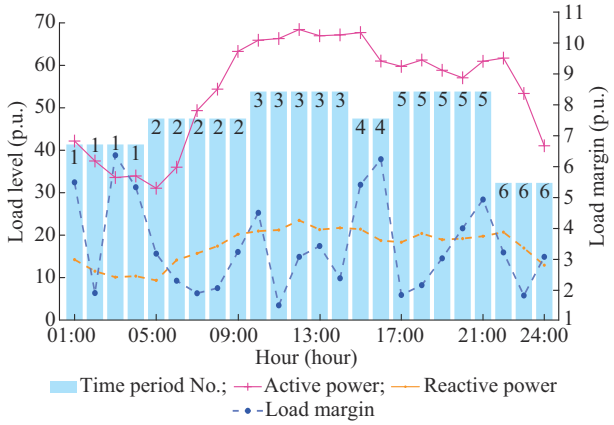

Fig. 7. Day-ahead load level and hourly load margins in worst scenario of IEEE 118-bus power system.

The 24 hours are partitioned into 4 time periods by the proposed methodology, as shown in Table II. The operations for NTO include switching out the line 114 at 01:00, switching out the line 185 and switching in the line 114 at 07:00, switching out the line 57 and switching in the line 185 at 17:00, and splitting bus 68 according to No. 190 splitting schemes, as shown in Table III. Hence, the total number of operations is 6. Note that Table III summarizes all bus-bar splitting schemes in the following study.

TABLE II
Time Partition and NTO Schemes of Proposed Methodology with Total Number of Operations of 6 in IEEE 118-bus Power System

Time partition		NTO scheme		
Period	Duration	No. of line switching-in	No. of line switching-out	Bus-bar splitting scheme No.
1	01:00-06:00		114	
2	07:00-16:00	114	185	
3	17:00-22:00	185	57	
4	23:00-24:00			+190

Note: "+" represents the execution of bus-bar splitting.

To evaluate the effectiveness of the proposed methodology, the load margins before and after NTOs in the 4 RSs of 24 hours are calculated by the continuation power flow method, as shown in Fig. 8, from which it can be concluded that the hourly load margins of 24 hours are all satisfied with the

desired requirement.

TABLE III
BUS-BAR SPLITTING SCHEMES

Case	Splitting bus-bar No.	Bus-bar splitting scheme No.	Bus-bar splitting scheme	
			No. of line connected on one bus	No. of line connected on another bus
118	17	65	21, 23, 178	22, 36, 39, L
	37	136	47, 51, 52	48, 50, 53, S
	68	190	107, 183	104, 126
	75	210	120, 185, L	115, 116, 117
	94	264	146, 147, L	145, 150, 155
3120	47	104	91, 92	95, 255
	1085	2840	1113, 1114	1176, L
	2576	9242	2275, 2261	2278, L
	2810	9560	2660, 3646	2693, 2702
	3100	10425	384, 2770	2628, 2768, 2780, 3671, L

Note: "L" represents the load branch on the splitting bus-bar, and "S" represents the shunt branch on the splitting bus-bar.

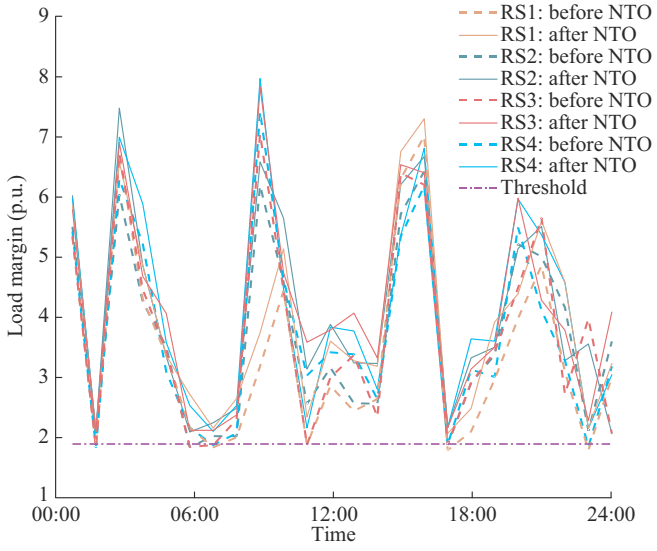

Fig. 8. Hourly load margins before and after NTOs in 4 RSs.

To show the effectiveness of the verification step proposed in stage III, this example is also tested by method M1. The time partition and NTO scheme are summarized in Table IV. It can be concluded that by method M1, the 24 hours are partitioned into 6 time periods, and the total number of operations is 9, which is more than that of the proposed methodology.

B. 3120-bus Power System

Assume that there are 6 PV stations at buses 1983, 1984, 1993, 2100, 2144, and 2146 and 6 wind generators at buses 2274, 2300, 2306, 2310, 2345, and 2349. The 55 load buses 430-440, 1100-1110, and 2800-2840 are divided into three different types of loads that vary according to the predicted load demand and 7 generators (at the buses 2791, 2794, 2797, 2803, 2814, 2823, and 2828) are scheduled to supply the increased load demand.

TABLE IV
TIME PARTITION AND NTO SCHEMES OF METHOD M1 WITH TOTAL NUMBER OF OPERATIONS OF 9

Time partition		NTO scheme		
Period	Duration	No. of line switching-in	No. of line switching-out	Bus-bar splitting scheme No.
1	01:00-04:00		114	
2	05:00-09:00	114	128	
3	10:00-14:00	128	26	
4	15:00-16:00	26	90	
5	17:00-21:00			
6	22:00-24:00	90		+190

Note: "+" represents the execution of bus-bar splitting.

The hourly load demands and load margins are shown in Fig. 9. Let $\lambda_{th}=6.2$ p.u.. In this example, 1844 transmission lines and 504 bus-bars (10488 bus-bar splitting schemes) are considered as the candidates for the NTO. As shown in Fig. 9, several hourly load margins do not meet the requirement.

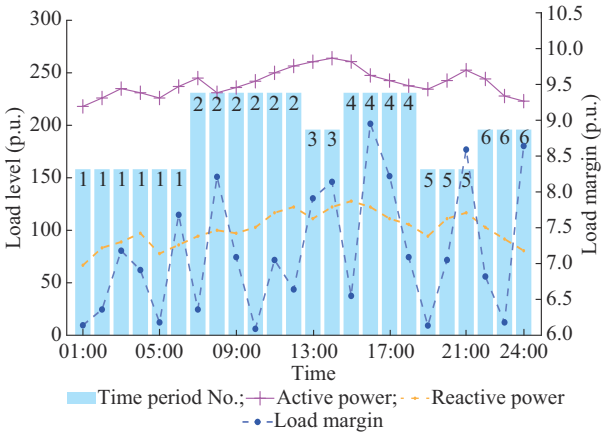

Fig. 9. Day-ahead load level and hourly load margins in worst scenario of 3120-bus power system.

After the proposed methodology is adopted, the 24 hours are partitioned into 4 time periods, as shown in Table V. The needed operations for the NTO include switching out the line 3654 at 01:00, switching in the line 3654 and switching out the line 2960 at 10:00, switching in the line 2960 and switching out the line 3060 at 19:00, and switching in the line 3060 and splitting the bus-bar 3100 according to the No. 10425 bus-bar splitting scheme, as shown in Table III. Hence, the total number of operations is 7. The hourly load margins in the 3 RSs with the lowest load margins before and after the NTO are calculated by the continuation power flow method, as shown in Fig. 10, from which it can be concluded that the hourly load margins of 24 hours are satisfied with the desired requirement.

To demonstrate the effectiveness of the proposed partition strategy, the simulation comparison is conducted between the proposed methodology and method M2. The results obtained by the two methods are summarized in Tables V and VI, respectively.

TABLE V
TIME PARTITION AND NTO SCHEMES OF PROPOSED METHODOLOGY WITH TOTAL NUMBER OF OPERATIONS OF 7 IN 3120-BUS POWER SYSTEM

Time partition		NTO scheme		
Period	Duration	No. of line switching-in	No. of line switching-out	Bus-bar splitting scheme No.
1	01:00-09:00		3654	
2	10:00-18:00	3654	2960	
3	19:00-22:00	2960	3060	
4	23:00-24:00	3060		+10425

Note: "+" represents the execution of bus-bar splitting.

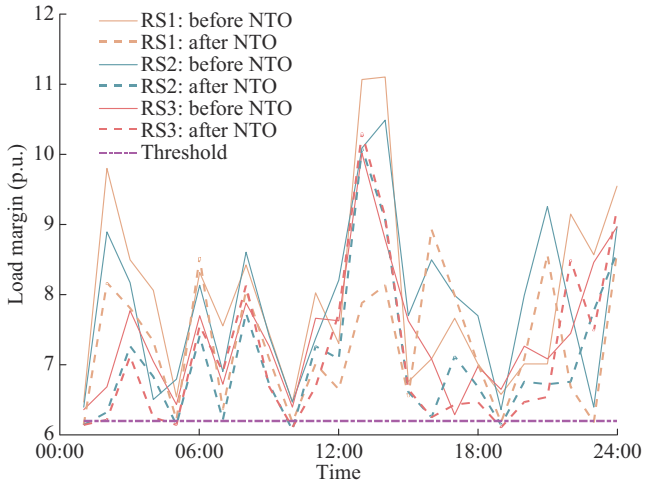

Fig. 10. Hourly load margins before and after NTOs in 3 RSs.

TABLE VI
TIME PARTITION AND NTO SCHEME OF METHOD M2 WITH TOTAL NUMBER OF OPERATIONS OF 11 IN 3120-BUS POWER SYSTEM

Time partition		NTO scheme		
Period	Duration	No. of line switching-in	No. of line switching-out	Bus-bar splitting scheme No.
1	01:00-04:00		64	
2	05:00-09:00	64	3410	
3	10:00-15:00	3410	546	
4	16:00-18:00	546	3541	
5	19:00-22:00	3541	135	
6	23:00-24:00	135		+10425

Note: "+" represents the execution of bus-bar splitting.

1) For the number of periods, 4 periods are identified by the proposed methodology, yet 6 periods are obtained by method M2, which are more than those of the proposed methodology.

2) For the number of operations, the network topology needs to be changed at 01:00, 10:00, 19:00, and 23:00 with the total number of operations of 7 by the proposed methodology. By method M2, the network topology needs to be changed at 01:00, 05:00, 10:00, 16:00, 19:00, and 23:00 with the total number of operations of 11, which is much more than that of the proposed methodology.

C. Comparison with Partition Method Based on Net Load

For comparison, the example on the IEEE 118-bus power system is tested by the proposed partition strategy based on the voltage changes in (18), (19) and the method M3. The day-ahead curves of wind power stations WT1-WT3 and PV power stations PV1-PV3 are shown in Fig. 11(a) and (b), respectively. Hence, the net load curve can be obtained, as shown in Fig. 11(c). The results obtained by method M3 are shown in Fig. 12.

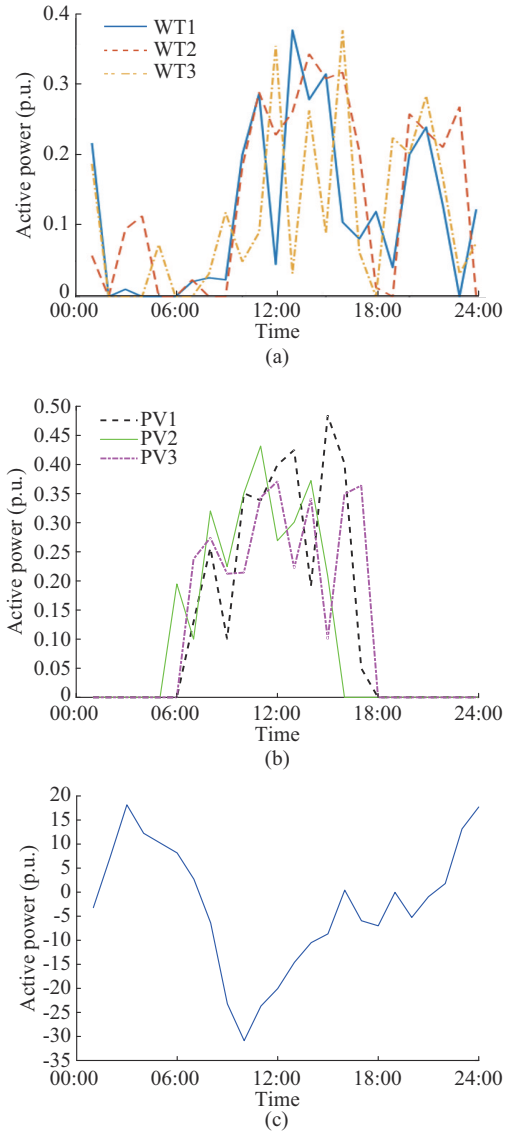

Fig. 11. Day-ahead curves of renewable energy sources and net load. (a) Wind power station. (b) PV power station. (c) Net load.

Comparing Fig. 7 and Fig. 12, it can be concluded that 6 periods are obtained by the proposed partition strategy, which include 01:00-04:00, 05:00-09:00, 10:00-14:00, 15:00-16:00, 17:00-21:00, and 22:00-24:00, whereas 8 periods are obtained by method M3. Furthermore, several short periods such as 01:00-02:00, 07:00-08:00, and 23:00-24:00 are identified by method M3. To identify the best NTO for these short periods, more calculations are requied.

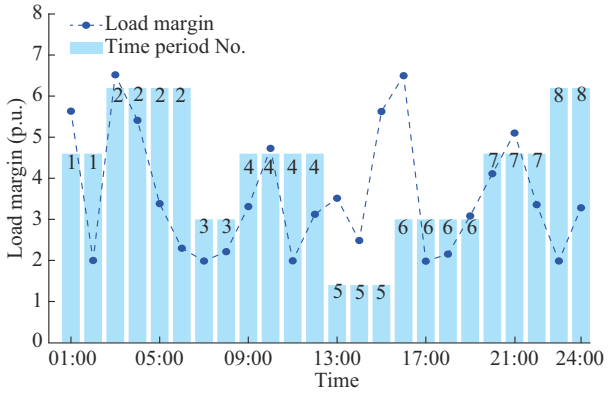

Fig. 12. Period partition results and load margins of method M3.

D. Comparison of Comprehensive NTO, Line Switching, and Bus-bar Splitting

To explore and show the effectiveness of the comprehensive NTO (including line switching and bus-bar splitting) on improving the voltage stability, two examples in the IEEE 118-bus power system and 3120-bus power system are conducted by the comprehensive NTO, line switching, and bus-bar splitting, respectively. The data of the two examples are the same as those in Section V-A and Section V-B. The simulation results of the two examples by line switching and bus-bar splitting are summarized in Table VII and Table VIII, respectively. The comprehensive NTO for the two examples are listed in Table II and Table V, respectively.

TABLE VII
SOLUTIONS BY LINE SWITCHING AND BUS-BAR SPLITTING OF IEEE 118-BUS POWER SYSTEM

Duration	Line switching		Bus-bar splitting scheme No.
	No. of line switching-in	No. of line switching-out	
01:00-06:00		114	+136
07:00-16:00	114	185	–136, +65
17:00-22:00	185	57	–65, +264
23:00-24:00	57	134, 65	–264, +190
Total number of operations	8		7

Note: "+" represents the execution of bus-bar splitting, and "–" represents the restoration of bus-bar splitting scheme.

TABLE VIII
SOLUTIONS BY LINE SWITCHING AND BUS-BAR SPLITTING OF 3120-BUS POWER SYSTEM

Duration of line switching	Line switching		Duration of bus-bar splitting	Bus-bar splitting scheme No.
	No. of line switching-in	No. of line switching-out		
01:00-09:00		3654	01:00-09:00	+2840
10:00-18:00	3654	2960	10:00-16:00	–2840, +9560
19:00-22:00	2960	3060	17:00-19:00	–9560, +104
23:00-24:00	3060	65, 423	20:00-22:00	–104, +9242
			22:00-24:00	–9242, +10425
Total number of operations	8			9

Note: "+" represents the execution of bus-bar splitting, and "–" represents the restoration of bus-bar splitting scheme.

It can be concluded that:

1) For the example of the IEEE 118-bus power system, 4 time periods are identified. For the line switching, the network topology needs to be altered at 01:00, 07:00, 17:00, and 23:00, and a total of 8 operations are needed to alter the network topology. For bus-bar splitting, the topology needs to be optimized according to the bus-bar splitting scheme Nos. 136, 65, 264, and 190, and a total of 7 operations are needed. However, from the results in Table II, only 5 operations are necessary for the comprehensive NTO, which are less than those of the line switching and bus-bar splitting.

2) For the example of the 3120-bus power system, 8 operations are needed by the line switching, and 9 operations are needed by the bus-splitting. However, from the results in Table V, only 7 operations are needed by the comprehensive NTO, which are less than those of the line switching and bus-bar splitting.

E. Effectiveness Under Heavy Loading Conditions

An example of the IEEE 118-bus power system is used to test the effectiveness of the proposed methodology under different loading conditions. In this test, 3 PV power stations are installed at buses 53, 54, and 55 and 3 wind generators are installed at buses 103, 104, and 105. The day-ahead active and reactive power loads and hourly load margins are shown in Fig. 13. Under this condition, the load margins in several hours are less than 1 p.u. (listed in Table IX), which shows the system is under the heavy loading condition and may cause voltage collapse at these hours, therefore set λ_{th} = 1 p.u. in this example.

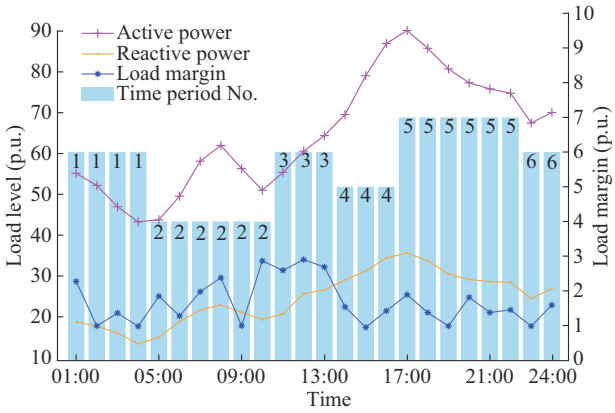

Fig. 13. Day-ahead load level and hourly load margins.

TABLE IX
INELIGIBLE LOAD MARGINS IN 4 RSS UNDER HEAVY LOADING CONDITION

RS 1		RS 2		RS 3		RS 4	
t	λ_t (p.u.)	t	λ_t (p.u.)	t	λ_t (p.u.)	t	λ_t (p.u.)
02:00	0.9978	04:00	0.9592	02:00	0.9968	02:00	0.9824
09:00	0.9918	14:00	0.9812	04:00	0.9280	04:00	0.9491
15:00	0.9561	15:00	0.7074	09:00	0.9883	09:00	0.9598
19:00	0.9359	23:00	0.9789	15:00	0.9483	15:00	0.9638
23:00	0.9366			19:00	0.9855	19:00	0.9849
				23:00	0.9645		

The results obtained by the proposed methodology are summarized in Table X, in which 4 periods are obtained and the total number of operations needed to alter the network topology is 7. The *P-V* curves before and after the NTO in the worst scenario at 02:00 and 23:00 are shown in Fig. 14, which shows that the load margin is satisfied with the desired requirement after the NTO. λ_{b2} and λ_{b23} are the load margins of base case (i.e., the pre-NTO power system) at 02:00 and 23:00, respectively; and λ_{a2} and λ_{a23} are the load margins of the post-NTO power system at the 02:00 and 23:00, respectively.

TABLE X
TIME PARTITION AND NTO SCHEMES BY PROPOSED METHODOLOGY WITH TOTAL NUMBER OF OPERATIONS OF 7

Time partition		NTO scheme		
Period	Duration	No. of line switching-in	No. of line switching-out	Bus-bar splitting scheme No.
1	01:00-08:00		185	
2	09:00-13:00	185	82	
3	14:00-18:00	82	30	
4	19:00-24:00	30		+210

Note: "+" represents the execution of bus-bar splitting.

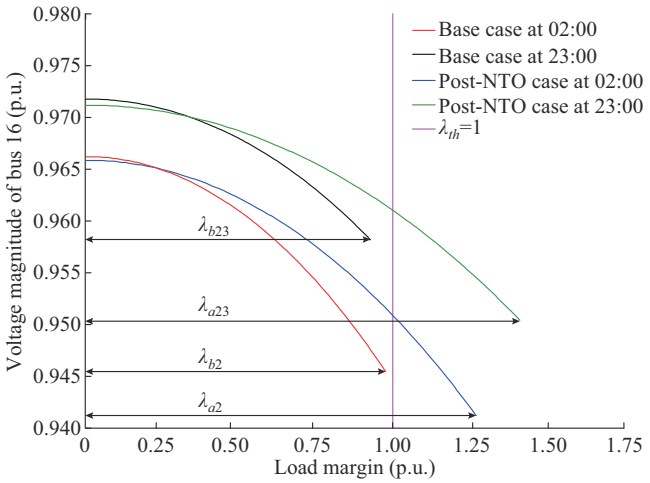

Fig. 14. *P-V* curves before and after NTO in worst scenario.

VI. CONCLUSION

This paper develops a DVNTO problem to improve the static day-ahead voltage stability of power systems by the comprehensive NTO with a minimum number of operations. A three-stage solution methodology is proposed to solve the problem. To flexibly mimic the change of topology by the NTO, a general NTO model is proposed and tailored for the screening task to quickly screen out those ineffective NTO schemes by a linear sensitivity-based method. To model the uncertainty, a scenario construction method is developed, specified for the static voltage stability problem, which can avoid the mis-elimination of the extreme scenario. To reduce the number of operations for NTO, a dynamic period partition strategy is presented. Extensive testing results on the IEEE 118-bus power system and 3120-bus power system demonstrated that the proposed methodology can effectively solve the proposed problem under different loading conditions with promising results.

Some of the future work is to further optimize the reactive power resources with the NTO to improve the voltage stability of power systems. Another relevant work is to improve the proposed problem by considering the other important constraints such as static stability and frequency stability constraints.

REFERENCES

[1] J. Zeng, F. Leng, X. Chen *et al*., "Implementation of high power digital-analog hybrid real-time simulation for modern power systems," *Automation of Electric Power Systems*, vol. 41, no. 8, pp. 166-171, Apr. 2017.
[2] Y. Lin, X. Zhang, J. Wang *et al*., "Voltage stability constrained optimal power flow for unbalanced distribution system based on semidefinite programming," *Journal of Modern Power Systems and Clean Energy*, vol. 10, no. 6, pp. 1614-1624, Nov. 2022.
[3] Z. Yun and X. Cui, "Online preventive control method for static voltage stability of large power grids," *IEEE Transactions on Power Systems*, vol. 35, no. 6, pp. 4689-4698, Nov. 2020.
[4] S. M. Mohseni-Bonab, A. Rabiee, and B. Mohammadi-Ivatloo, "Voltage stability constrained multi-objective optimal reactive power dispatch under load and wind power uncertainties: a stochastic approach," *Renewable Energy*, vol. 85, pp. 598-609, Jan. 2016.
[5] E. A. Leonidaki, D. P. Georgiadis, and N. D. Hatziargyriou, "Decision trees for determination of optimal location and rate of series compensation to increase power system loading margin," *IEEE Transactions on Power Systems*, vol. 21, no. 3, pp. 1303-1310, Aug. 2006.
[6] S. S. Ladhani, "Criteria for load control when considering static stability limits," in *Proceedings of IEEE PES General Meeting*, San Francisco, USA, Jun. 2005, pp. 1558-1562.
[7] A. Merlin and H. Bach, "Search for a minimum-loss operating spanning tree configuration for an urban power distribution system," in *Proceedings of Power Systems Computer Conference*, Cambridge, UK, Sept. 1975, pp. 1-5.
[8] A. A. Mazi, B. F. Wollenberg, and M. H. Hesse, "Corrective control of power system flows by line and bus-bar switching," *IEEE Transactions on Power Systems*, vol. 1, no. 3, pp. 258-264, Jul. 1986.
[9] W. Shao and V. Vittal, "Corrective switching algorithm for relieving overloads and voltage violations," *IEEE Transactions on Power Systems*, vol. 20, no. 4, pp. 1877-1885, Nov. 2005.
[10] B. Zhao, Z. Hu, Q. Zhou *et al*., "Optimal transmission switching to eliminate voltage violations during light-load periods using decomposition approach," *Journal of Modern Power Systems and Clean Energy*, vol. 7, no. 2, pp. 297-308, Mar. 2019.
[11] M. Khanabadi, H. Ghasemi, and M. Doostizadeh, "Optimal transmission switching considering voltage security and *N*–1 contingency analysis," *IEEE Transactions on Power Systems*, vol. 28, no. 1, pp. 542-550, Feb. 2013.
[12] W. Zhang, B. Hu, K. Xie *et al*., "Short-term transmission maintenance scheduling considering network topology optimization," *Journal of Modern Power Systems and Clean Energy*, vol. 10, no. 4, pp. 883-893, Jul. 2022.
[13] K. W. Hedman, R. P. O'Neill, E. B. Fisher *et al*., "Optimal transmission switching with contingency analysis," *IEEE Transactions on Power Systems*, vol. 24, no. 3, pp. 1577-1586, Aug. 2009.
[14] E. B. Fisher, R. P. O'Neill, and M. C. Ferris, "Optimal transmission switching," *IEEE Transactions on Power Systems*, vol. 23, no. 3, pp. 1346-1355, Aug. 2008.
[15] H. Haghighat, "Loading margin calculation with line switching: a decomposition method," *International Journal of Electrical Power & Energy Systems*, vol. 64, pp. 104-111, Jan. 2015.
[16] L. Wang and H. D. Chiang, "Toward online line switching for increasing load margins to static stability limit," *IEEE Transactions on Power Systems*, vol. 31, no. 3, pp. 1744-1751, May 2016.
[17] L. Wang and H. D. Chiang, "Toward online bus-bar splitting for increasing load margins to static stability limit," *IEEE Transactions on Power Systems*, vol. 32, no. 5, pp. 3715-3725, Sept. 2017.
[18] H. Hua, T. Liu, C. He *et al*., "Day-ahead scheduling of power system with short-circuit current constraints considering transmission switching and wind generation," *IEEE Access*, vol. 9, pp. 110735-110745, Aug. 2021.

[19] M. A. Khorsand and K. W. Hedman, "Day-ahead corrective transmission topology control," in *Proceeding of 2014 IEEE PES General Meeting*, National Harbor, USA, Jul. 2014, pp. 1-5.
[20] S. Golshannavaz, S. Afsharnia, and F. Aminifar, "Smart distribution grid: optimal day-ahead scheduling with reconfigurable topology," *IEEE Transactions on Smart Grid*, vol. 5, no. 5, pp. 2402-2411, Sept. 2014.
[21] Y. Li, B. Hu, K. Xie *et al*., "Day-ahead scheduling of power system incorporating network topology optimization and dynamic thermal rating," *IEEE Access*, vol. 7, pp. 35287-35301, Mar. 2019.
[22] T. Lan, Z. Zhou, W. Wang *et al*., "Stochastic optimization for AC optimal transmission switching with generalized Benders decomposition," *International Journal of Electrical Power & Energy Systems*, vol. 133, p. 107140, Dec. 2021.
[23] F. Qiu and J. Wang, "Chance-constrained transmission switching with guaranteed wind power utilization," *IEEE Transactions on Power Systems*, vol. 30, no. 3, pp. 1270-1278, May 2015.
[24] D. Sarkar, A. De, C. K. Chanda *et al*., "Kruskal's maximal spanning tree algorithm for optimizing distribution network topology to improve voltage stability," *Electric Power Components and Systems*, vol. 43, no. 17, pp. 1921-1930, Oct. 2015.
[25] A. M. Othman, A. A. El-Fergany, and A. Y. Abdelaziz, "Optimal reconfiguration comprising voltage stability aspect using enhanced binary particle swarm optimization algorithm," *Electric Power Components and Systems*, vol. 43, no. 14, pp. 1656-1666, Aug. 2015.
[26] J. M. Peñaranda and M. C. Pacis, "Stochastic optimal transmission switching considering voltage stability index with distributed generation uncertainty," in *Proceedings of 2022 IEEE 14th International Conference on Humanoid*, *Nanotechnology*, *Information Technology*, *Communication and Control*, *Environment*, *and Management*, Boracay Island, Philippines, Dec. 2022, pp. 1-6.
[27] M. Chakravorty and D. Das, "Voltage stability analysis of radial distribution networks," *International Journal of Electrical Power & Energy Systems*, vol. 23, no. 2, pp. 129-135, Feb. 2001.
[28] C. Wang, L. Wang, X. Deng *et al*., "Scenario-based line switching for enhancing static voltage stability with uncertainty of renewables and loads," *International Journal of Electrical Power & Energy Systems*, vol. 145, p. 108653, Feb. 2023.
[29] F. Capitanescu and L. Wehenkel, "Redispatching active and reactive powers using a limited number of control actions," *IEEE Transactions on Power Systems*, vol. 26, no. 3, pp. 1221-1230, Aug. 2011.
[30] H. Gao, W. Ma, Y. Xiang *et al*., "Multi-objective dynamic reconfiguration for urban distribution network considering multi-level switching modes," *Journal of Modern Power Systems and Clean Energy*, vol. 10, no. 5, pp. 1241-1255, Sept. 2022.
[31] C. Wang and Y. Gao, "Dynamic reconfiguration of distribution network based on optimal fuzzy C-means clustering and improved chemical reaction optimization," *Proceedings of the CSEE*, vol. 34, pp. 1682-1691, Apr. 2014.
[32] Y. Hong and Y. Luo, "Optimal var control considering wind farms using probabilistic load-flow and gray-based genetic algorithms," *IEEE Transactions on Power Delivery*, vol. 24, no. 3, pp. 1441-1449, Jul. 2009.
[33] S. Li and H. D. Chiang, "Continuation power flow with nonlinear power injection variations: a piecewise linear approximation," *IEEE Transactions on Power Systems*, vol. 23, no. 4, pp. 1637-1643, Nov. 2008.
[34] N. R. Pal and J. C. Bezdek, "On cluster validity for the fuzzy C-means model," *IEEE Transactions on Fuzzy Systems*, vol. 3, no. 3, pp. 370-379, Aug. 1995.
[35] X. Li, K. Wang, L. Liu *et al*., "Application of the entropy weight and TOPSIS method in safety evaluation of coal mines," *Procedia Engineering*, vol. 26, pp. 2085-2091, Jan. 2011.
[36] Y. Fu and H. D. Chiang, "Toward optimal multiperiod network reconfiguration for increasing the hosting capacity of distribution networks," *IEEE Transactions on Power Delivery*, vol. 33, no. 5, pp. 2294-2304, Oct. 2018.
[37] W. Wang and Y. Zhang, "On fuzzy cluster validity indices," *Fuzzy Sets and Systems*, vol. 158, no. 19, pp. 2095-2117, Oct. 2007.
[38] D. W. Kim, K. H. Lee, and D. Lee, "On cluster validity index for estimation of the optimal number of fuzzy clusters," Pattern Recognition, vol. 37, no. 10, pp. 2009-2025, Apr. 2004.
[39] H. D. Chiang, C. Wang, and A. J. Flueck, "Look-ahead voltage and load margin contingency selection functions for large-scale power systems," *IEEE Transactions on Power Systems*, vol. 12, no. 1, pp. 173-180, Aug. 1997.
[40] University of Washington. (2023, Jan.). Power systems test case archive. [Online]. Available: http://www.ee.washington.edu/research/pstca/
[41] International Renewable Energy Agency. (2023, Feb.). Historical data of renewable energy sources. [Online]. Available: https://www.irena.org/
[42] California Independent System Operator. (2023, Jan.). Electric load data. [Online]. Available: https://www.caiso.com/

Dingli Guo received the B.S. degree in Qilu University of Technology, Jinan, China, in 2021. He is currently pursuing the M.S. degree in the School of Electrical and Electronic Engineering, Shandong University of Technology, Zibo, China. His research interest includes the voltage stability analysis and controls of power systems.

Lei Wang received the Ph.D. degree in electrical engineering from Tianjin University, Tianjin, China, in 2015. She is currently an Associate Professor in the School of Electrical and Electronic Engineering, Shandong University of Technology, Zibo, China. Her research interests include nonlinear system theory and computation, power system stability and control, and optimization theory and applications.

Ticao Jiao received the B.S. degree from the School of Mathematics, Institute of Automation,Qufu, China, the M.S. degree from Qufu Normal University, Qufu, China, in 2008 and 2012, respectively, and the Ph.D. degree in control theory and control engineering from the Nanjing University of Science and Technology, Nanjing, China, in 2016. Since 2016, he has been a Professor with the School of Electrical and Electronic Engineering, Shandong University of Technology, Zibo, China. His research interests include stochastic systems, switched systems, and impulsive systems.

Ke Wu received the B.S. degree in electrical engineering and automation from Shandong University of Technology, Zibo, China, in 2022. He is currently pursuing the M.S. degree in electrical engineering at Shandong University of Technology. Her research interests include dynamic line rating and power system voltage stability.

Wenjing Yang received the B.S. degree in electrical engineering and automation from East China Jiaotong University, Nanchang, China, in 2021. She is currently pursuing the M.S. degree in electrical engineering at Shandong University of Technology, Zibo, China. Her research interests include power system stability and control.